

Chandra HIGH ENERGY GRATING OBSERVATIONS OF THE Fe K α LINE CORE IN TYPE 2 SEYFERT GALAXIES: A COMPARISON WITH TYPE 1 NUCLEI

X. W. SHU¹, T. YAQOOB², J. X. WANG¹

Draft version September 25, 2018

ABSTRACT

We present a study of the core of the Fe K α emission line at ~ 6.4 keV in a sample of type II Seyfert galaxies observed by the *Chandra* High Energy Grating (HEG). The sample consists of 29 observations of 10 unique sources. We present measurements of the Fe K α line parameters with the highest spectral resolution currently available. In particular, we derive the most robust intrinsic line widths for some of the sources in the sample to date. We obtained a weighted mean FWHM of 2000 ± 160 km s⁻¹ for 8 out of 10 sources (the remaining sources had insufficient signal-to-noise). From a comparison with the optical emission-line widths obtained from spectropolarimetric observations, we found that the location of Fe K α line-emitting material is a factor of $\sim 0.7 - 11$ times the size of the optical BLR. Furthermore, compared to 13 type I AGNs for which the best Fe K α line FWHM constraints were obtained, we found no difference in the FWHM distribution or the mean FWHM, and this conclusion is independent of the central black hole mass. This result suggests that the bulk of the Fe K α line emission may originate from a universal region at the same radius with respect to the gravitational radius, $\sim 3 \times 10^4 r_g$ on average. By examining the correlation between the Fe K α luminosity and the [O IV] line luminosity, we found a marginal difference in the Fe K α line flux between type I and type II AGNs, but the spread in the ratio of L_{Fe} to $L_{\text{[OIV]}}$ is about two orders of magnitude. Our results confirm the theoretical expectation that the Fe K α emission-line luminosity cannot trivially be used as a proxy of the intrinsic AGN luminosity, unless a detailed comparison of the data with proper models is applied.

Subject headings: galaxies: active – line: profile – X-rays: galaxies

1. INTRODUCTION

Both type I and type II active galactic nuclei (AGN) are known to exhibit a narrow (FWHM $< 10,000$ km s⁻¹) Fe K α fluorescent emission line at ~ 6.4 keV in their X-ray spectrum (e.g. Sulentic et al. 1998; Lubiński & Zdziarski 2001; Weaver, Gelbord, & Yaqoob 2001; Perola et al. 2002; Yaqoob & Padmanabhan 2004 (hereafter YP04); Levenson et al. 2002, 2006; Jiang et al. 2006; Winter et al. 2009; Shu, Yaqoob & Wang 2010, hereafter paper I). The line profile of the Fe K α core is important for probing its origin and it can provide unique information on the dynamics and physical state of the line-emitting region (Yaqoob et al. 2001, 2003, 2007). While it is widely accepted that the narrow Fe K α line cores are produced in cold, neutral matter far from the nucleus, the exact location and distribution of the line-emitting gas still remain uncertain (see Paper I, and references therein). Nandra (2006) first examined the relation between the Fe K α and optical H β line widths, which can potentially give a direct indication of the location of the Fe K α line-emitting region relative to the optical broad-line region (BLR). However, the results were ambiguous, and the data allow for an origin of the Fe K α line anywhere from the outer regions of an accretion disk, the BLR, and a parsec-scale torus. Meanwhile, Bianchi et al. (2008) reported a meaningful comparison

between the Fe K α and H β line widths in NGC 7213, and found the FWHM of both lines are consistent with each other (~ 2500 km s⁻¹), implying a BLR origin of the Fe K α emission line. Using the high-energy grating (HEG) on the *Chandra* HETGS (*High Energy Transmission Grating Spectrometer*, see Markert et al. 1995), which affords the best spectral resolution currently available in the Fe K band (at 6.4 keV is ~ 39 eV, or ~ 1860 km s⁻¹ FWHM), in Paper I we presented a more thorough and comprehensive study of the Fe K α line core emission in a large sample of type I Seyfert galaxies (see also YP04). We measured the intrinsic width of the narrow Fe K α line core and obtained a weighted mean of FWHM = 2060 ± 230 km s⁻¹. A comparison with the optical emission-line widths suggested that there may not be a universal location of the Fe K α line-emitting region relative to the BLR, consistent with the results of Nandra (2006). Our results in fact showed that the location of the Fe K α line emitter relative the BLR appears to be different from source to source.

However, one must be cautious in explaining the origin of the narrow Fe K α core, especially for measurements made with instruments that have lower spectral resolution than the *Chandra* HETGS (e.g., see Liu et al. 2010 for NGC 5548). The uncertainty in the intrinsic line width measurements is usually large, and part of the narrow component may have a contribution from an underlying broad line in some (if not all) unobscured AGNs (e.g., Lee et al. 2002; YP04; Nandra 2006). However, in cases when the narrow Fe K α core is unresolved even with the *Chandra* HEG, such contamination is not an issue, and from the upper limits on the line widths we can place

¹ CAS Key Laboratory for Research in Galaxies and Cosmology, Department of Astronomy, University of Science and Technology of China, Hefei, Anhui 230026, P. R. China, xwshu@mail.ustc.edu.cn, jxw@ustc.edu.cn

² Department of Physics and Astronomy, Johns Hopkins University, Baltimore, MD 21218, yaqoob@pha.jhu.edu

strongly constrains on the origin of the intrinsically narrow Fe $K\alpha$ line core (see Paper I). In the paradigm of the unification model (Antonucci 1993), the narrow Fe $K\alpha$ line emission in type II AGNs is expected to be produced in the same material as in type I nuclei. Therefore, one of the things that we would like to know is whether there is any systematic difference in the origin of the Fe $K\alpha$ line in type I and type II AGNs. In addition, for a given geometry and model, one would expect a particular relation between the equivalent width (EW) of the Fe $K\alpha$ line, N_H , and the orientation of line-emitting structure (e.g., Murphy & Yaqoob 2009; Ikeda, Teramshima, & Awaki 2009; Yaqoob et al. 2010; Brightman & Nandra 2011). Thus a comparison of Fe $K\alpha$ emission-line luminosities and EWs in type I AGNs versus type II AGNs can potentially offer basic tests of some of the predictions of AGN unification scenarios.

In this paper, we present a study of the narrow Fe $K\alpha$ emission line in a sample of type II AGNs observed with the *Chandra HETGS*. The observations and spectral fitting are described in Section 2. In Section 3, we present the results for the properties of the core of the narrow Fe $K\alpha$ emission line and their implications. In Section 4, we summarize our results and findings. Throughout this paper, we adopt a cosmology of $\Omega_M = 0.3$, $\Omega_\Lambda = 0.7$, and $H_0 = 70 \text{ km s}^{-1} \text{ Mpc}^{-1}$.

2. OBSERVATIONS AND SPECTRAL FITTING

Our study is based on *Chandra HETGS* observations of AGNs, which were in the *Chandra* public archive as of 2010 Aug 1. In Paper I, we presented a study of the properties of the Fe $K\alpha$ line emission in a sample of predominantly type I AGNs. In this paper, we expand the sample of AGN in Paper I to include type II sources by simple modifications of the selection criteria. One is to lift any constraints on the column density (i.e., there now no selection on column density), and the other is to lower the acceptance threshold for the total number of counts in the HEG spectra. The sample in Paper I was composed of the least complex spectra due to a maximum column density criterion, and a threshold of a total number of HEG counts of 1,500. The reader is referred to Paper I for the details of the remaining selection criteria, which were not changed. Lowering the signal-to-noise threshold was necessary because the larger equivalent widths of the Fe $K\alpha$ line for heavily absorbed sources result in useful constraints for sources that are weaker than those with smaller equivalent widths. With the two modified selection criteria, we end up with a sample that now includes both type I and type II AGN, as well as intermediate types. The present paper reports on the results of an analysis of 29 observations of the 10 sources in the new, larger sample that were not included in Paper I. Not surprisingly, the sources in the present paper are all classified as type II in NED (including NGC 1275, also known as 3C 84 and Perseus A, which lies at the center of a rich cluster of galaxies, and has a peculiar optical emission-line spectrum with two distinct narrow emission-line systems, e.g., Conselice et al. 2001).

We note that the relationship between the optical classification of an AGN as type I to type II and the X-ray absorption properties is not always clear cut, so the sample in Paper I included some AGN that were not type I. In particular, Paper I included NGC 5506, MCG –5-

23-16, and NGC 2110, which are type 1.9 AGN. When comparing the results for the type II AGN in the present paper, we simply refer to the intermediate Seyfert types in Paper I as type I for convenience (this is more of a reflection of the relative simplicity of the X-ray spectrum). We note that since the publication of Paper I, 15 new observations of two of the AGN in Paper I (NGC 4051 and Akn 564) have been made public. The new observations have been analyzed and this information has been incorporated into the comparisons between the results in Paper I and the present paper.

The *Chandra HETGS* consists of two grating assemblies, a High-Energy Grating (HEG) and a Medium-Energy Grating (MEG), and it is the HEG that achieves the highest spectral resolution. The MEG has only half of the spectral resolution of the HEG and less effective area in the Fe K band, so our study will focus on the HEG data. Out of the 10 unique sources, 8 were observed more than once: namely NGC 4945, the Circinus galaxy, NGC 6240, NGC 1068, Centaurus A, NGC 4388, NGC 4258 and NGC 1275. The remaining two sources that were observed only once are NGC 4057 and Mrk 3. In order to obtain the highest precision measurements of the Fe $K\alpha$ emission-line parameters, in particular for the width of the line, we concentrate on the analysis of the co-added spectra for the sources with multiple observations. We checked that for sources observed more than once, the count rates variations are very small (less than 10%). Therefore, in this study we report only the results of time-averaged spectroscopy. The mean HEG counts rates ranged from $0.006 \pm 0.001 \text{ ct/s}$ for the weakest source (NGC 4945) to $0.792 \pm 0.004 \text{ ct/s}$ for the brightest source (Centaurus A). The exposure time ranged from $\sim 10 \text{ ks}$ to $\sim 170 \text{ ks}$ per observation, and the largest net exposure time from summed data from observations of the same source was $\sim 440 \text{ ks}$ (NGC 1068). Details of the 29 observations used in this paper are given in Table 1.

The *Chandra* data for the sample were reduced and HEG spectra were made as described in Yaqoob et al. (2003) and YP04. We used only the first orders of the grating data (combining the positive and negative arms). Further details of all of the observations can be found in the *Chandra* data archive at <http://cda.harvard.edu/chaser/>. Higher-level products, including lightcurves and spectra for each observation can be found in the databases *HotGAS* (<http://hotgas.pha.jhu.edu>), and *TGCat* (<http://tgcate.mit.edu/>). Background was not subtracted since it is negligible over the energy range of interest (e.g. see Yaqoob et al. 2003). Note that the systematic uncertainty in the HEG wavelength scale is $\sim 433 \text{ km s}^{-1}$ ($\sim 11 \text{ eV}$) at 6.4 keV ³.

The spectra were analyzed using the spectral-fitting package XSPEC (Arnaud 1996). Since we are interested in utilizing the highest possible spectral resolution available, we used spectra binned at 0.0025 \AA , and this amply oversamples the HEG resolution (0.012 \AA FWHM). The *C*-statistic was used for minimization. All model parameters will be referred to the source frame. Our method is simply to fit a simple absorbed continuum plus

³ <http://space.mit.edu/CXC/calib/hetgcal.html>

Gaussian emission-line model over the 3–10 keV band for each spectrum, to avoid the influence of the complex absorption and many soft X-ray emission lines below 3 keV (e.g., Levenson et al. 2006), while providing enough high-energy coverage to fit the continuum. Galactic absorption was not included for any of the sources because such small column densities have little effect above 3 keV. For NGC 4258 and NGC 1275, the Fe K α line was only weakly detected: C decreased by 3.4 and 2.0, respectively, when a narrow, unresolved emission line at 6.4 keV was added to the continuum. These figures correspond to detections at less than 95% confidence, and less than 90% confidence for NGC 4258 and NGC 1275 respectively (for the addition of one free parameter). For these two sources we were therefore only able to obtain constraints on the line flux (and not on the line centroid energy and line width), so the Gaussian model had one free parameter. Note that a significant Fe K α emission line has been detected in NGC 4258 by *Suzaku* and *XMM-Newton* (Yamada et al. 2009; Reynolds et al. 2009), with $EW=45 \pm 17$ eV and $EW=53 \pm 19$ eV, respectively, which is consistent with the upper limit of 32 eV (at 90% confidence) obtained by the *Chandra* HEG.

Thus, except for the two cases mentioned above, for the remaining spectra the Gaussian model component had three free parameters and there were a total of six free parameters in the model, namely the power-law continuum slope (Γ), the overall normalization of the power-law continuum, the column density, N_H , the centroid energy of the Gaussian emission-line component, E_0 , its flux, $I_{\text{Fe K}}$, and its width, $\sigma_{\text{Fe K}}$. The approach of using an oversimplified continuum model is necessitated by the limited bandpass of the HEG data ($\sim 3 - 10$ keV) but since we are interested in the narrow core of the Fe K α emission line, at the spectral resolution of the HEG, this is not restrictive. As we will show in Section 3.1, in cases when the Fe K α line was significantly detected, its centroid energy as well as its intrinsic width can be well-measured by the *Chandra* HEG. We note that even for cases where we can obtain a reliable measure of the Fe K α line FWHM, the true line width may be less than the FWHM deduced from our simplistic model-fitting because there may be blending from an unresolved Compton-shoulder component (e.g., Matt 2002; Yaqoob & Murphy 2011). However, this artificial broadening is not an issue for the line parameters of the high signal-to-noise ratio HEG observations reported here. For example, although Circinus has one of the most robust detections of a Compton-shoulder component (e.g., Bianchi et al. 2002), it has the smallest FWHM measure among the HEG sample. Obviously, use of such an empirical model means that we should not assign a physical meaning to Γ and N_H . We emphasize that our approach in the present paper is to perform a very simple *empirical* analysis in order to obtain robust measurements of the basic narrow Fe K α line core parameters that are not dependent on details of how the continuum is modeled. A realistic physical model of the continuum and the analysis of the soft X-ray spectral components is beyond the scope of this work and will be presented elsewhere.

3. RESULTS AND DISCUSSIONS

3.1. Spectroscopy in the Fe K Band

Figure 1 shows the HEG spectrum for each source in the Fe K region, corrected for instrumental efficiency and cosmological redshift. The spectra are binned at 0.01 Å, similar to the HEG FWHM spectral resolution of 0.012 Å. The statistical uncertainties correspond to 68% confidence Poisson errors, which we calculated using equations (7) and (14) in Geherls (1986) that approximate the upper and lower errors respectively. For sources which were observed more than once, the time-averaged spectra are shown. It can be seen that in some spectra, emission lines from different ionized species of Fe are evident, in addition to the narrow Fe K α line at ~ 6.4 keV, but the latter is always the strongest line. Although in the present paper we are concerned only with the Fe K α line core centered at ~ 6.4 keV, overlaid on the spectra in Fig. 1 are vertical dashed lines marking the expected positions of the Fe xxv He-like triplet lines (the two intercombination lines are shown separately), Fe xxvi Ly α , Fe I K β , and the neutral Fe K-shell threshold absorption-edge energy. The values adopted for these energies were from NIST2 (He-like triplet); Pike et al. 1996 (Fe xxvi Ly α); Palmeri et al. 2003 (Fe I K β), and Verner et al. 1996 (Fe K edge). We emphasize that the emission from higher ionization states of Fe has little effect on the measurements of the intrinsic width of the Fe K α line. For example, for NGC 1068 the spectral plot in the Fe K band shows a broad emission feature on the blue side of the Fe K α line peak, which is probably due to multiple species of ionic Fe. The occurrence of highly ionized Fe emission lines in AGN X-ray spectra has been noted since the *ASCA* observations, and they are extensively studied recently with *XMM-Newton* and *Suzaku* (e.g., Bianchi et al. 2005; Fukazawa et al. 2011). However, we can confirm from the 99% confidence contour of Fe K α line intensity versus FWHM (Figure 2), that the Fe K α line width is still well-constrained (less than ~ 3500 km s $^{-1}$). This conclusion is also consistent with the physical width of the narrow core of the Fe K α line in the spectral plot that is apparent simply from visual inspection.

The best-fitting Fe K α emission-line parameters for each spectrum are shown in Table 2. We do not give the best-fitting values of Γ or N_H in Table 2 because the values derived using the simplistic continuum model are not physically meaningful but are simply parameterizations. We obtained a weighted mean line-center energy of 6.397 ± 0.001 keV for the 24 observations of 8 sources. At 99% confidence (for three free parameters), none of the AGNs has a line centroid energy greater than ~ 6.41 keV, indicating that the line-emitting matter is cold and essentially neutral, consistent with results presented in Paper I for a sample of type I AGNs. Here, and hereafter, for the calculation of the weighted mean of any quantity with asymmetric errors, we simply assumed symmetric errors, using the largest 68% confidence error from spectral fitting.

3.2. The Intrinsic Width of the Fe K α Line Emission

From our spectral fits (Table 2) and the joint confidence contours of Fe K α line intensity versus FWHM (Figure 2 and 3), we found that at 99% confidence, the *Chandra* HEG resolves the narrow component of the Fe K α emission in 8 out of 10 sources. The

weighted mean FWHM of the Fe $K\alpha$ line cores is $200 \pm 160 \text{ km s}^{-1}$. The fact that this mean is approximately equal to the HEG FWHM spectral resolution is not indicative of a calibration bias. This is supported by the fact that the FWHM of the Fe $K\alpha$ line in Circinus is *less* than the HEG FWHM at a confidence level of greater than 99%. In addition, the spectral resolution for gratings does not degrade with time because it is determined principally by spatial dispersion, and the resolution is well-established from bright Galactic sources with narrow lines (<http://space.mit.edu/CXC/calib/hetgcal.html>). Note that the weighted mean value is consistent with the straight mean of the FWHM, of $2510 \pm 160 \text{ km s}^{-1}$. The measurements of the intrinsic width of the line can potentially be used to constrain the location of the medium responsible for the core of the Fe $K\alpha$ emission line (e.g., Yaqoob et al. 2001). Comparing the Fe $K\alpha$ line FWHM with that of the optical broad emission lines (e.g., $H\alpha$ and/or $H\beta$ lines) can give a direct indication of the location of the Fe $K\alpha$ line-emitting region relative to the optical broad-line region (Nandra 2006, Bianchi et al. 2008, Paper I). To place limits on the location of the Fe $K\alpha$ emitter relative to the BLR, we compiled from the literature the width of optical broad emission line from spectro-polarimetric observations for five sources in our sample, and the values of the $H\alpha$ or $H\beta$ FWHM are listed in Table 2. The near-infrared broad lines have not been taken into account in the present paper, as they are possibly produced in a region that differs from the BLR in density, and/or in the amount of extinction (e.g., Ramos Almeida et al. 2008; Landt et al. 2008). However, in cases where there is no spectropolarimetric data at all, the FWHM of near-infrared lines might still yield some useful information⁴.

Figure 3 shows the 99% confidence contours of the Fe $K\alpha$ line intensity versus the *ratio* of the Fe $K\alpha$ FWHM to optical line FWHM. We found that at the two-parameter 99% confidence level, the FWHM ratio lies in the range of $\sim 0.3 - 1.2$. At 99% confidence, the Fe $K\alpha$ line widths in 3 out of 5 sources are less than that of optical lines, suggesting that the observed Fe $K\alpha$ emission is not likely produced in a BLR where the optical lines are produced. The remaining two sources (NGC 4388 and NGC 1068) could have consistent width for both lines. This would be expected in at least one source, NGC 4388, which is known to have significant column density variations (Elvis et al. 2004), if its BLR acts as absorber and emitter seen in the X-ray band. In fact, there is now significant evidence that the BLR may act as an X-ray absorber, like in the cases of NGC 1365 and NGC 7582 (e.g., Risaliti et al. 2005; Bianchi et al. 2009). However, if the BLR is obscured by a fully covering column density greater than $\sim 5 \times 10^{23} \text{ cm}^{-2}$ (as in the cases of NGC 4507, Mrk 3 and the Circinus) any Fe $K\alpha$ line component from the BLR will be greatly diminished, or undetectable. If the BLR is obscured by such a large column density, the only way it would be possible to observe an Fe $K\alpha$ line component from the

BLR is if the BLR is not fully covered. The fact that the Fe $K\alpha$ line width of Compton-thick source NGC 1068 is consistent with that of the polarized $H\beta$ line (within 99% errors) could be simply attributed to the large error in the Fe $K\alpha$ line width. Alternatively, this could indicate that the heavy obscuration which blocks the BLR has comparable size with that of the BLR.

Since Keplerian velocities are inversely proportional to the square root of the orbit size, the observed distribution of the ratio of the Fe $K\alpha$ to optical line FWHM implies that the Fe $K\alpha$ line-emitting region size could be a factor $\sim 0.7 - 11$ times larger than the optical line-emitting region. We obtained a weighted mean of 0.57 ± 0.05 for the ratios of the Fe $K\alpha$ line FWHM to the optical line FWHM, corresponding to the Fe $K\alpha$ line-emitting region being, on average, ~ 3 times the size of BLR. However, for AGNs in general, there may be no universal location of the Fe $K\alpha$ line-emitting region within a factor of $\sim 1-10$ times size of BLR. However, as we will show later, the Fe $K\alpha$ line emitter may be associated with a universal location in terms of gravitational radius (r_g , where $r_g = GM_{\text{BH}}/c^2$). If the Fe $K\alpha$ line emission has a significant contribution from the putative obscuring torus that is required by AGN unification models, our results show that the size-scale of the torus may be smaller than traditionally thought. Note that Gaskell, Goosmann, & Klimek (2008) argue that there is considerable observational evidence that the BLR itself has a toroidal structure, and that there may be no distinct boundary between the BLR and the classical parsec-scale torus.

One of the interesting things that we can investigate is whether the material responsible for producing the narrow Fe $K\alpha$ line in type II AGNs systematically differs from that in type I objects. Of the AGNs in the sample reported in Paper I, we identified thirteen type I AGNs (including 3 moderately obscured sources with weak broad Balmer lines, formally classified as intermediate type AGNs) that provided the very best statistical constraints on the Fe $K\alpha$ line FWHM (as indicated by the two-parameter confidence contours of line flux versus FWHM; see Figure 6 in Paper I). The weighted mean FWHM of the Fe $K\alpha$ core is $2170 \pm 220 \text{ km s}^{-1}$, in good agreement with the measurement for type II AGNs in the present sample. However, we found a slightly larger FWHM of the Fe $K\alpha$ line ($3620 \pm 220 \text{ km s}^{-1}$) for type I AGNs if the straight mean is used, but as we will show below, it may be due to a bias towards the measurements with lower quality data. We show in Figure 4 the distribution of Fe $K\alpha$ line FWHM for the current sample (solid line), compared with the thirteen type I AGNs in Paper I (dashed line). It can be seen that both histograms are not Gaussian and are not strongly peaked. In addition, we found that the measurement of the FWHM in one AGN (namely MCG -6-30-15) deviated significantly from the distribution of the rest of the sources. From our empirical analysis, we obtained $\text{FWHM} = 11880^{+4650}_{-4030} \text{ km s}^{-1}$ (see Paper I) for this object, and the corresponding 90% confidence lower limit (for three free parameters) is $\sim 6000 \text{ km s}^{-1}$. Note that MCG -6-30-15 has the strongest and broadest Fe $K\alpha$ line yet observed in an AGN. The larger FWHM obtained from our empirical analysis could be attributed to the Fe $K\alpha$ core from

⁴ We searched in the literature and found that only one source, NGC 6240, has NIR broad-line $\text{Br}\alpha$ measurement reported, with $\text{FWHM} = 1800 \pm 200 \text{ km/s}$ (Cai et al. 2010). This value is consistent with the width of the Fe K line at 99% confidence.

underlying disk-line component, and/or a complex continuum (e.g., Miller et al. 2008). Note that Young et al. (2005) analyzed the *Chandra* HEG spectrum by using more complex models including both disk-line and narrow Fe K α core emission, and obtained an FWHM < 4700 km s⁻¹ for the narrow component, which is consistent with those from the other sources in our sample. However, as the narrow Fe K α line EW is relatively low (~ 60 eV, see Paper I), we cannot tell whether the line profile is affected by the complex continuum, or whether it is intrinsically broader than the other AGNs. Future X-ray missions, such as *Astro-H*, which has much higher spectral resolution, will help to measure the true profile of the narrow Fe K α emission line in this object. Even considering the one AGN mentioned above, there is not a significant difference in the distribution of FWHM for the two subsamples. A Kolmogorov-Smirnov (K-S) test shows that the probability that the type I (including MCG -6-30-15) and type II AGNs are drawn from the same parent population is 0.83. Therefore, it appears that there is no difference in the origin of the Fe K α line in type I and type II AGNs, which is consistent with the predictions of the unification model.

Figure 5 shows the relationship between the Fe K α line FWHM and the black hole mass (see Table 2 caption for references). Open and solid circles denote type I and type II AGNs, respectively. We see that all FWHM values, within the statistical errors, are consistent with a constant, independent of the mass of black hole. Assuming that the line originates in material that is in a virialized orbit around the black hole, we can estimate the distance, r , of the line-emitting material to the black hole using the relation $GM_{\text{BH}} = r\langle v^2 \rangle$. Assuming that the velocity dispersion is related to FWHM velocity as $\langle v^2 \rangle = \frac{3}{4}v_{\text{FWHM}}^2$ (Netzer et al. 1990), we can obtain $r = (4c^2)/(3v_{\text{FWHM}}^2)r_g$, where $r_g = GM/c^2$. Using the weighted mean of FWHM ~ 2000 km s⁻¹, we find that the $r \sim 3 \times 10^4 r_g$, larger than the typical size of the BLR (e.g., Peterson et al. 2004). Therefore, our results seem to support the bulk of the Fe K α line production arising from a region that appears to be located at a universal distance with respect to the gravitational radius, which is controlled by central black hole mass. Note that Nandra (2006) also examined the relation between the FWHM of Fe K α line and the black hole mass, but their results were ambiguous. The reason why they did not find the result that we found is possibly due to the fact that some of the sources in their sample had only poor quality and/or problematic Fe K α line-width measurements. Including such sources could have obscured the underlying result that r/r_g may be the key factor that determines the location of the line-emitting region. However, it is important to note that even with superb *Chandra* HEG spectral resolution, there may be blending from a Compton-shoulder component and/or multiple low ionization states of Fe (e.g., Yaqoob & Murphy 2011), so that the true line width may be less than the FWHM deduced from our simplistic model-fitting.

3.3. What can we learn from the Fe K α Line Emission?

From a theoretical point of view, the flux or luminosity of the Fe K α line (L_{Fe}) is nontrivial to calculate, as it depends on a number of factors, including geometry,

orientation, covering factor, element abundance, and column density of the line-emitting material. Using Monte Carlo simulations of a toroidal X-ray reprocessor model, Murphy & Yaqoob (2009, see also Yaqoob et al. 2010) showed that geometrical and inclination-angle effects become important for $N_H \gtrsim 10^{23}$ cm⁻² for the observed EW and line flux. For a given covering factor and set of element abundances, a toroidal structure with a column density of greater than $\sim 5 \times 10^{24}$ cm⁻², observed at an edge-on inclination could produce an Fe K α emission line flux that is an order of magnitude or more weaker than a face-on orientation (Yaqoob et al. 2010). In particular, the Fe K α line luminosity is not simply a linear function of N_H , and it has a maximum value for a column density in the range $\sim 3 - 8 \times 10^{23}$ cm⁻², depending on the inclination angle. Therefore, the Fe K α line luminosity cannot be trivially used to measure the intrinsic AGN luminosity (L_{AGN}). The relation between L_{Fe} and L_{AGN} is more complicated than we would expect from optically-thin matter, and it is strongly model dependent, and in particular it depends on covering factor, inclination angle and column density. We emphasize that the column density for producing the Fe K α line does not refer to the line-of-sight value, but rather to a value that corresponds to the angle-averaged flux over all incident X-ray continuum radiation (see Murphy & Yaqoob 2009).

Recently, Liu & Wang (2010) confirmed that L_{Fe} and L_{AGN} are not simply related. They compared the narrow Fe K α line emission between type I and type II AGNs, using data obtained with *XMM-Newton*, and found that statistically, the Fe K α line luminosities in Compton-thin and Compton thick type II AGNs are about 2.7 and 5.6 times lower than that in type I sources, respectively. They therefore proposed that different correction factors should be applied if one uses the Fe K α line emission to estimate the AGN's intrinsic luminosity. To examine the relation between L_{Fe} and L_{AGN} for our *Chandra* grating sample, we plot in Figure 6 (upper panel) the Fe K α line luminosity (L_{Fe}), versus the [O IV] 25.89 μm line luminosity ($L_{[\text{OIV}]}$), which is claimed to be an intrinsic AGN luminosity indicator, see Meléndez et al. 2008a). The type II AGNs are shown with solid circles, while open circles represent 24 type I AGNs for which the [O IV] line luminosity is available from literature. Solid stars denote tentative Compton-thick sources, based on previously reported measurements of N_H (e.g., Treister, Urry & Virani 2009, and references therein). The right-hand panel shows the distribution of L_{Fe} for both type I (dotted line) and type II (solid line) AGNs. It can be seen that the distribution of the Fe K α line luminosity in type II AGNs is not significantly different from that in type I AGNs. A K-S test shows the probability that both samples were drawn from the same parent population is 0.21. However, when normalizing the Fe K α line luminosity by the [O IV] line luminosity ($L_{\text{Fe}}/L_{[\text{OIV}]}$), the lower panel of Figure 6), we find a marginal difference in the distributions of the $L_{\text{Fe}}/L_{[\text{OIV}]}$ ratio for type I and type II AGNs, but the significance level is not high (at 93% confidence), possibly due to the small size of the current *Chandra* grating sample. The dotted and dashed horizontal lines show the means of $L_{\text{Fe}}/L_{[\text{OIV}]}$ for Liu & Wang's type I and type II subsamples, respectively. It seems that the distribution of the $L_{\text{Fe}}/L_{[\text{OIV}]}$ ratio for

our *Chandra* grating sample shows a similar pattern as Liu & Wang’s sample. However, we note that there is significant overlap between the type I and type II AGNs with intermediate values of the $L_{\text{Fe}}/L_{[\text{OIV}]}$ ratio (see also Liu & Wang 2010, Figure 6), suggesting the complex dependencies of the Fe $K\alpha$ line emission on the geometry and physical properties of the line-emitting material. In the context of a toroidal geometry (e.g., Murphy & Yaqoob 2009), the sources in the overlap region of the $L_{\text{Fe}}/L_{[\text{OIV}]}$ plot may however indicate that they constitute a selected distribution of N_H and inclination angle (e.g., Circinus galaxy, Yang et al. 2009), but a larger sample is required to make a detailed comparison.

Although in our study we cannot determine some of the critical parameters of the Fe $K\alpha$ line emitter, such as global covering factor, N_H , and the inclination angle of the X-ray reprocessor, we can still make interesting statements from the plot of $L_{[\text{OIV}]}$ vs. $L_{\text{Fe}}/L_{[\text{OIV}]}$. It is apparent that the ratio of $L_{\text{Fe}}/L_{[\text{OIV}]}$ appears to have a dispersion of 2 to 3 orders of magnitude or so. Regardless of AGN type, the sources located at the top end of the $L_{\text{Fe}}/L_{[\text{OIV}]}$ ratio distribution are expected to be those objects that are observed at a face-on, or near face-on, inclination angle, with moderate N_H ($\sim 0.5 - 2 \times 10^{24} \text{ cm}^{-2}$). The sources located in the region of the lowest values of $L_{\text{Fe}}/L_{[\text{OIV}]}$ should correspond to cases with higher N_H and higher inclination angles. We note that the source with the lowest ratio of $L_{\text{Fe}}/L_{[\text{OIV}]}$ is the prototypical Seyfert 2 galaxy NGC 1068, for which an edge-on orientation of the torus and a high, Compton-thick column density has already been suggested in literature (e.g., Pounds et al. 2006, and references therein).

4. SUMMARY

We have presented an empirical analysis of 29 observations of the narrow core of the Fe $K\alpha$ emission line in 10 type II AGNs using *Chandra* HEG data. The Fe $K\alpha$ line was significantly detected, and its parameters (line centroid energy, intrinsic width and line flux) were well-measured, in 8 out of 10 sources. The centroid energy of Fe $K\alpha$ line is found to be strongly peaked around ~ 6.4 keV, indicating an origin in cool, neutral matter, consistent with the results of Paper I for a sample of type I AGNs.

We obtained a weighted mean value of FWHM = $2000 \pm 160 \text{ km s}^{-1}$ for the intrinsic Fe $K\alpha$ line width. For five sources with spectro-polarimetric observations, we constructed 99% confidence, two-parameter contours of line flux versus the ratio of the width of the Fe $K\alpha$ line

to the width of the H β line. We found that the 99% confidence bounds on the ratio of the X-ray line width to the optical line width lies in the range $\sim 0.3 - 1.2$, suggesting that contributions to the flux of the core of the Fe $K\alpha$ line are allowed from a region that is within a factor $\sim 0.7 - 11$ times the radius of the optical BLR. Compared to 13 type I AGNs with sufficiently high quality Fe $K\alpha$ line-width measurements (reported in paper I), we found no difference in the distribution between the Fe $K\alpha$ FWHM in type I and type II AGNs, and this conclusion is independent of the central black mass. This result suggests there may be a universal location for the bulk of the Fe $K\alpha$ line emission with respect to the gravitational radius (r_g). However, these conclusions are subject to the caveat that derivation of the true velocity width of the Fe $K\alpha$ line core requires a realistic physical model, and this will be the subject of future work.

Having isolated the narrow core of the Fe $K\alpha$ line with the best available spectral resolution, we also presented measurements of the line luminosity of the Fe $K\alpha$ core, and examined its relation to the intrinsic AGN luminosity (i.e., by means of the $L_{[\text{OIV}]}$ indicator). We found a marginal difference in the distribution of the Fe $K\alpha$ emission-line luminosity between type I and type II AGNs, but the significance level is not high, and the spread in the $L_{\text{Fe}}/L_{[\text{OIV}]}$ is about 2 orders of magnitude. Although the complex dependencies of the Fe $K\alpha$ emission-line parameters upon the covering factor, inclination angle and column density, prevent trivial use of the Fe $K\alpha$ luminosity as a proxy of the intrinsic AGN’s luminosity, the *Chandra* results presented here will provide an important and new supplement to additional X-ray spectroscopy with a broader bandpass. A detailed comparison of the data for the Fe $K\alpha$ line and the continuum with appropriate models will then yield more robust constraints on the intrinsic AGN luminosity and the physical parameters of the X-ray processor.

We thank E. Moran for helpful discussions on the spectropolarimetric observations of NGC 4507. X.W.S. thanks the support from China postdoctoral foundation. We acknowledge support from Chinese National Science Foundation (Grant No. 10825312), and the Fundamental Research Funds for the Central Universities (Grant No. WK2030220004, WK2030220005). This research made use of the HEASARC online data archive services, supported by NASA/GSFC. This research has made use of the NASA/IPAC Extragalactic Database (NED) which is operated by the Jet Propulsion Laboratory, California Institute of Technology, under contract with NASA. The authors are grateful to the *Chandra* instrument and operations teams for making these observations possible.

REFERENCES

- Antonucci, R. 1993, ARA&A, 31, 473
 Arnaud, K. A., 1996, Astronomical Data Analysis Software and Systems V, eds. Jacoby, G., & Barnes, J., p. 17, ASP Conference Series, Vol. 101
 Bian W., & Gu Q. 2007, ApJ, 657, 159
 Bianchi S., Matt, G., & Fiore, F. et al. 2002, A&A, 396, 793
 Bianchi S., La Franca F., Matt G., Guainazzi M., Jiménez-Bailón E., Longinotti A. L., Nicastro F., Pentericci L., 2008, MNRAS, 389, 52
 Bianchi, S., Piconcelli, E., Chiaberge, M. et al. 2009, ApJ, 695, 781
 Brightman M., & Nandra K., 2011, MNRAS, in press (arXiv:1012.3345)
 Cai, H. B., Shu, X. W., Wang, J. X., & Zheng, Z. Y. 2010, RAA, 10, 427
 Conselice, C. J., Gallagher, J. S., Wyse, R. F. G. 2001, AJ, 122, 2281
 Elvis, M., Risaliti, G., Nicastro, F. et al. 2004, ApJ, 615, 25
 Fukazawa, Y. Hiragi, K., Mizuno, M. et al. 2011, ApJ, 727, 19
 Gaskell C. M., Goosmann R. W., Klinek E. S., 2008, MmSAI, 79, 1090
 Gehrels, N. 1986, ApJ, 303, 33

- Greenhill L. J., Moran J. M., Herrnstein J. R. et al. 1997, ApJ, 481, L23
- Ikeda S., Awaki, H., & Terashima Y. 2009, ApJ, 692, 608
- Jiang, P., Wang, J. X., & Wang, T. G. 2006, ApJ, 644, 725
- Landt, H., Bentz, M. C., Ward, M. J. et al. 2008, ApJS, 174, 282
- Lee J. C., Iwasawa K., Houck J. C. et al. 2002, ApJ, 570, L47
- Levenson N. A., Krolik J. H., Zycki, P. Y. et al. 2002, ApJ, L81
- Levenson N. A., Heckman T. M., Krolik J. H., Weaver K. A., Zycki P. T., 2006, ApJ, 648, 111
- Liu Y., Elvis, M., McHardy, I. M. et al. 2010, ApJ, 710, 1228
- Liu T., & Wang, J. X. 2010, ApJ, 725, 238
- Lubiński P., Zdziarski A. A., 2001, MNRAS, 323, L37
- Marconi, A., Capetti, A., Axon, D. J. et al. 2001, ApJ, 549, 915
- Markert T. H., Canizares C. R., Dewey D., McGuirk M., Pak C., Shattenburg M. L., 1995, Proc. SPIE, 2280, 168
- Matt, G. 2002, MNRAS, 337, 147
- Meléndez, M., et al. 2008a, ApJ, 682, 94
- Meléndez, M., et al. 2008b, ApJ, 689, 95
- Miller L., Turner T. J. & Reeves J. N. 2008, A&A, 483, 437
- Moran E. C., Barth A. J., Kay L. E., & Filippenko A. V. 2000, ApJ, 540, L73
- Murphy K., Yaqoob T., 2009, MNRAS, 397, 1549
- Nandra K., 2006, MNRAS, 368, L62
- Netzer, H., et al. 1990, ApJ, 353, 108
- Nishiura S., & Taniguchi Y. 1998, ApJ, 499, 134
- Oliva E., Marconi A., Cimatti A., Alighieri S. D. 1998, A&A, 329, 21
- Palmeri P., Mendoza C., Kallman T. R., Bautista M. A., Melendez M., 2003, A&A, 410, 359
- Perola G. C., Matt G., Cappi M., Fiore F., Guainazzi M., Maraschi L., Petrucci P. O., Piro, L., 2002, A&A, 389, 802
- Peterson B. M., Ferrarese L., Gilbert K. M. et al. 2004, ApJ, 613, 682
- Pike C. D., Phillips K. J. H., Lang J. et al. 1996, ApJ, 464, 487
- Pounds K., & Vaughan S. 2006, MNRAS, 368, 707
- Ramos Ameida, C. et al. 2008, ApJ, 680, L17
- Reynolds C. S., Nowak M. A., & Markoff S. et al. 2009, ApJ, 691, 1159
- Risaliti, G., Elvis, M., Fabbiano, G., Baldi, A., & Zezas, A. 2005, ApJ, 623, L93
- Shu X. W., Yaqoob T. & Wang J. X. 2010, ApJS, 187, 581 (Paper I)
- Sulentic J. W., Marziani P., Zwitter T., Calvani M., Dultzin-Hacyan, D., 1998, ApJ, 501, 54
- Tecza M., Genzel R., Tacconi L. J. et al. 2000, ApJ, 537, 178
- Treister E., Urry C. M., & Virani S. 2009, ApJ, 696, 110
- Tremaine S., Gebhardt K., Bender R. et al. 2002, ApJ, 574, 740
- Verner D. A., Ferland G. J., Korista K. T., Yakovlev D. G., 1996, ApJ, 465, 487
- Weaver K. A., Gelbord J., Yaqoob T., 2001, ApJ, 550, 261
- Winter L. M., Mushotzky R. F., Reynolds C. S., Tueller J., 2009, ApJ, 690, 1322
- Woo J. H., & Urry C. M. 2002, ApJ, 579, 530
- Yamada S., Itoh T., Makishima K., & Nakazawa, K. 2009, PASJ, 61, 309
- Yang Y., Wilson A. S., Matt G., Terashima Y., Greenhill L. J. 2009, ApJ, 691, 131
- Yaqoob T., George I. M., Nandra K., Turner T. J., Serlemitsos P. J., Mushotzky R. F., 2001, ApJ, 546, 759
- Yaqoob T., George I. M., Kallman T. R., Padmanabhan U., Weaver. K. A., Turner T. J., 2003, ApJ, 596, 85
- Yaqoob T., Padmanabhan U., 2004, ApJ, 604, 63 (YP04)
- Yaqoob T., Murphy K. D., Griffiths R. E. et al. 2007, PASJ, 59, 283
- Yaqoob T., & Murphy, K. D. 2011, MNRAS, 412, 277
- Yaqoob T., & Murphy, K. D., Miller, L. & Turner, T. J. 2010, MNRAS, 401, 411
- Young S. et al. 1996, MNRAS, 281, 1206
- Young A. J., Lee J. C., Fabian A. C., Reynolds C. S., Gibson R. R., Canizares C. R., 2005, ApJ, 631, 733

Figure 1

Chandra HEG spectra in the Fe K band for sources in our sample. For eight AGN which were observed more than once, the time-averaged spectra are shown. The data are binned at 0.01\AA , comparable to the HEG spectral resolution, which is 0.012\AA FWHM. The data are combined from the -1 and $+1$ orders of the grating. The spectra have been corrected for instrumental effective area and cosmological redshift. Note that these are *not* unfolded spectra and are therefore independent of any model that is fitted. The statistical errors shown correspond to the 1σ (asymmetric) Poisson errors, which we calculated using equations (7) and (14) in Geherls (1986) that approximate the upper and lower errors respectively. The solid line corresponds to a continuum model fitted over the 3–10 keV range, as described in the text (Section 2). The vertical dotted lines represent (from left to right), the rest energies of the following: Fe I $K\alpha$, Fe XXV forbidden, two intercombination lines of Fe XXV, Fe XXV resonance, Fe XXVI Ly α , Fe I $K\beta$, and the Fe K edge.

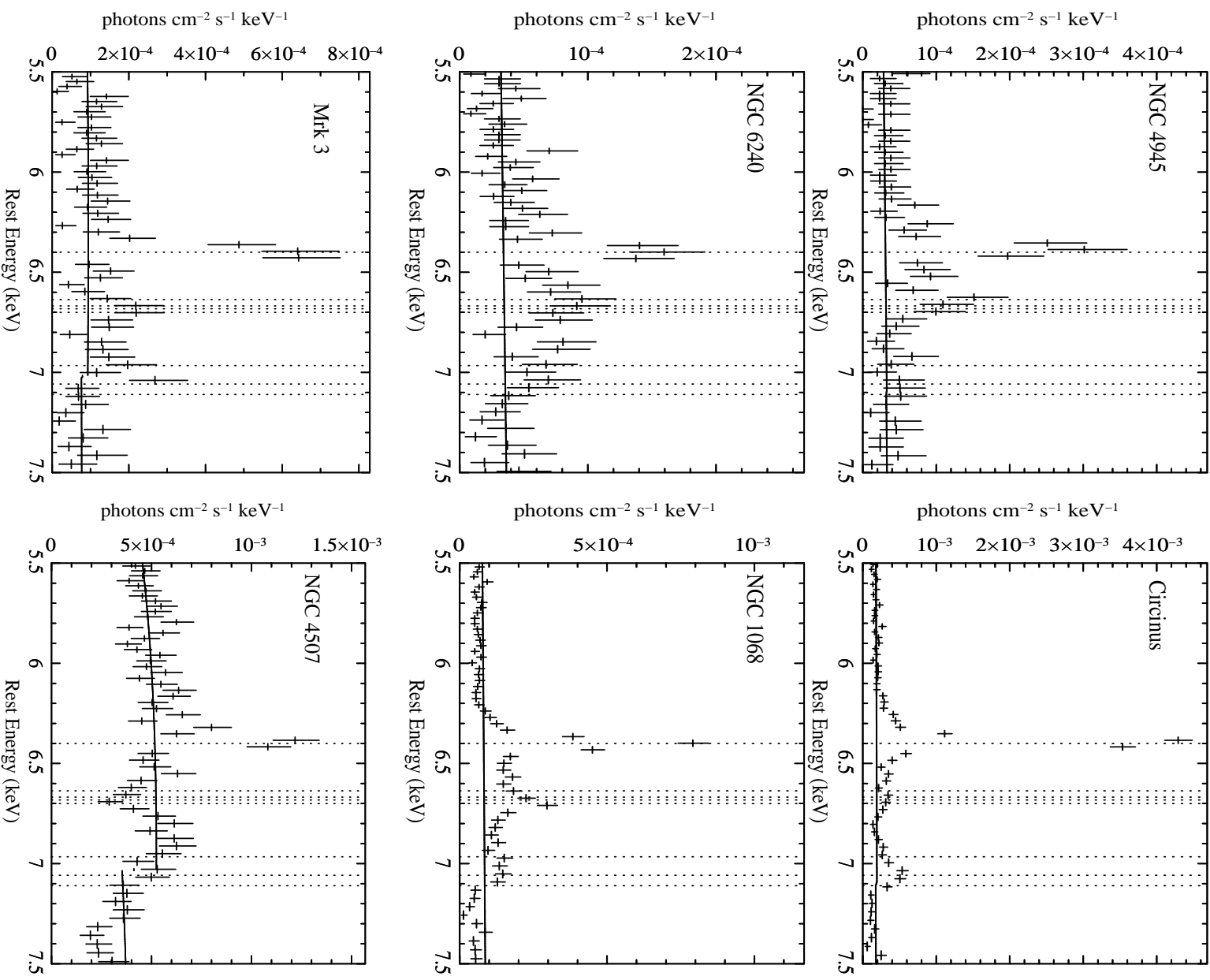
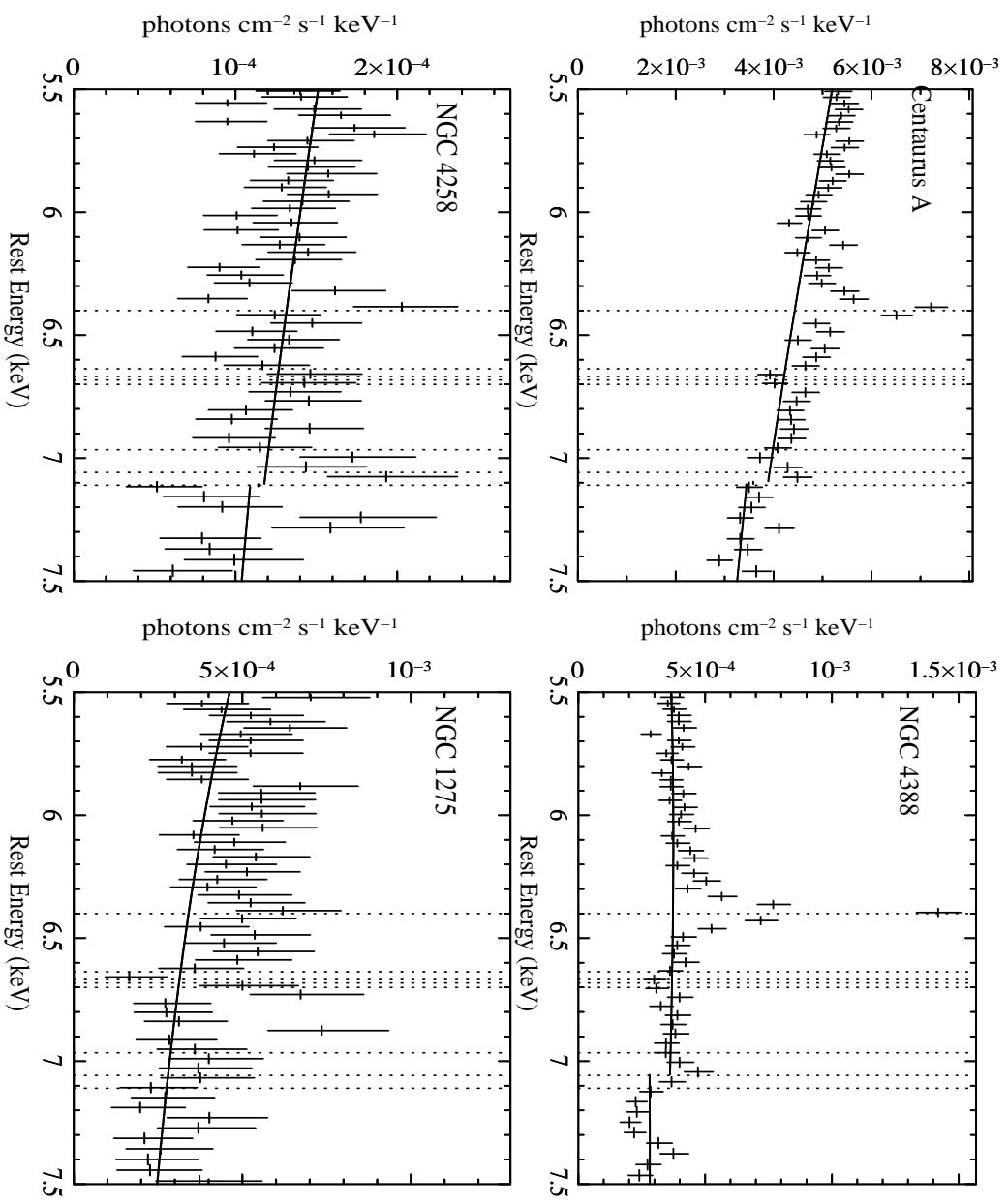


Fig. 1.—

Fig. 1. — *continued*

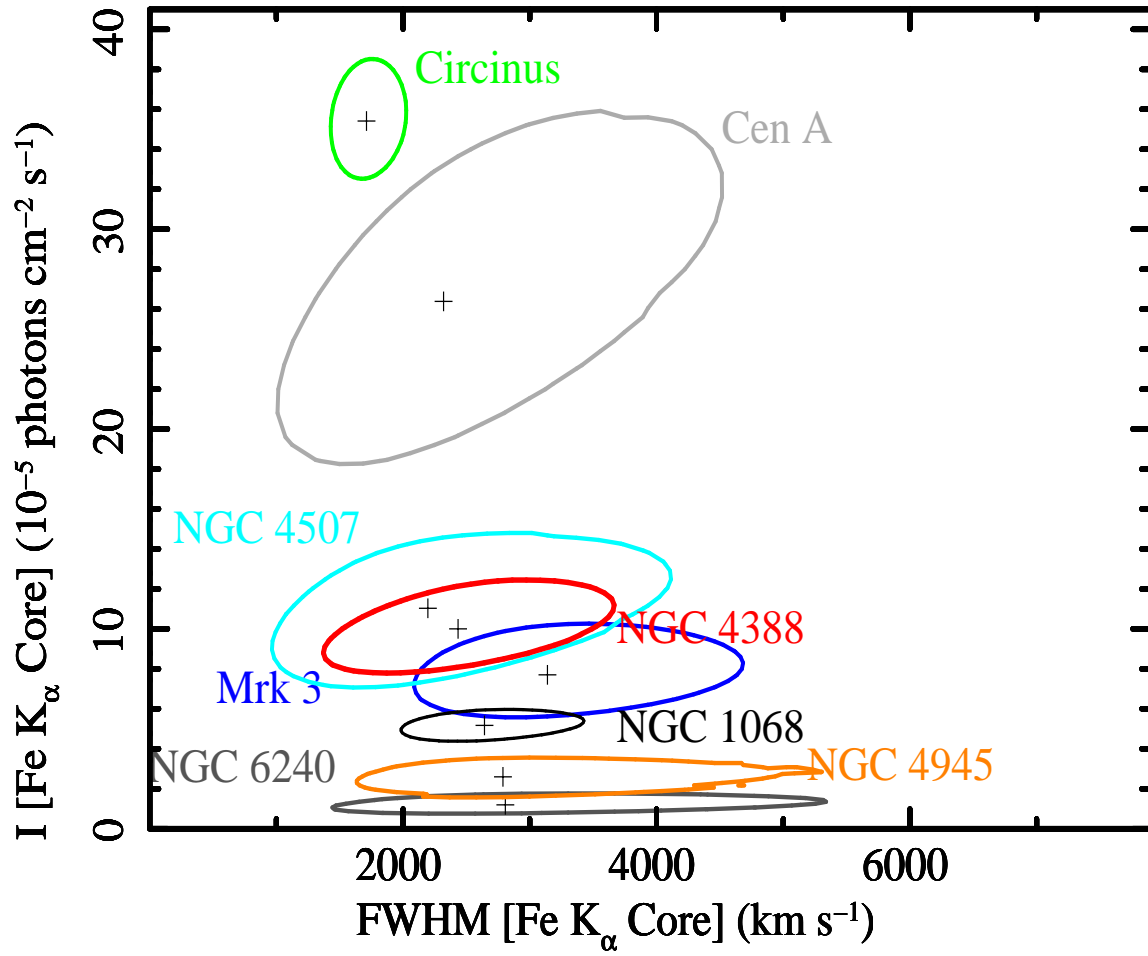


FIG. 2.— Joint 99% confidence contours of the Fe $K\alpha$ emission line intensity vs. velocity width (FWHM), obtained from Gaussian fits to the line as described in the text, for eight AGNs: NGC 4945 (orange), Circinus (green), NGC 6240 (light grey), NGC 1068 (black), Mrk 3 (blue), NGC 4507 (light blue), Centarus A (dark grey) and NGC 4388 (red). The well-constrained contours (see also Fig. 3) suggest that our single-Gaussian fits are picking up an intrinsic narrow component at ~ 6.4 keV, and the effects of any complex continuum components on the line parameters are small.

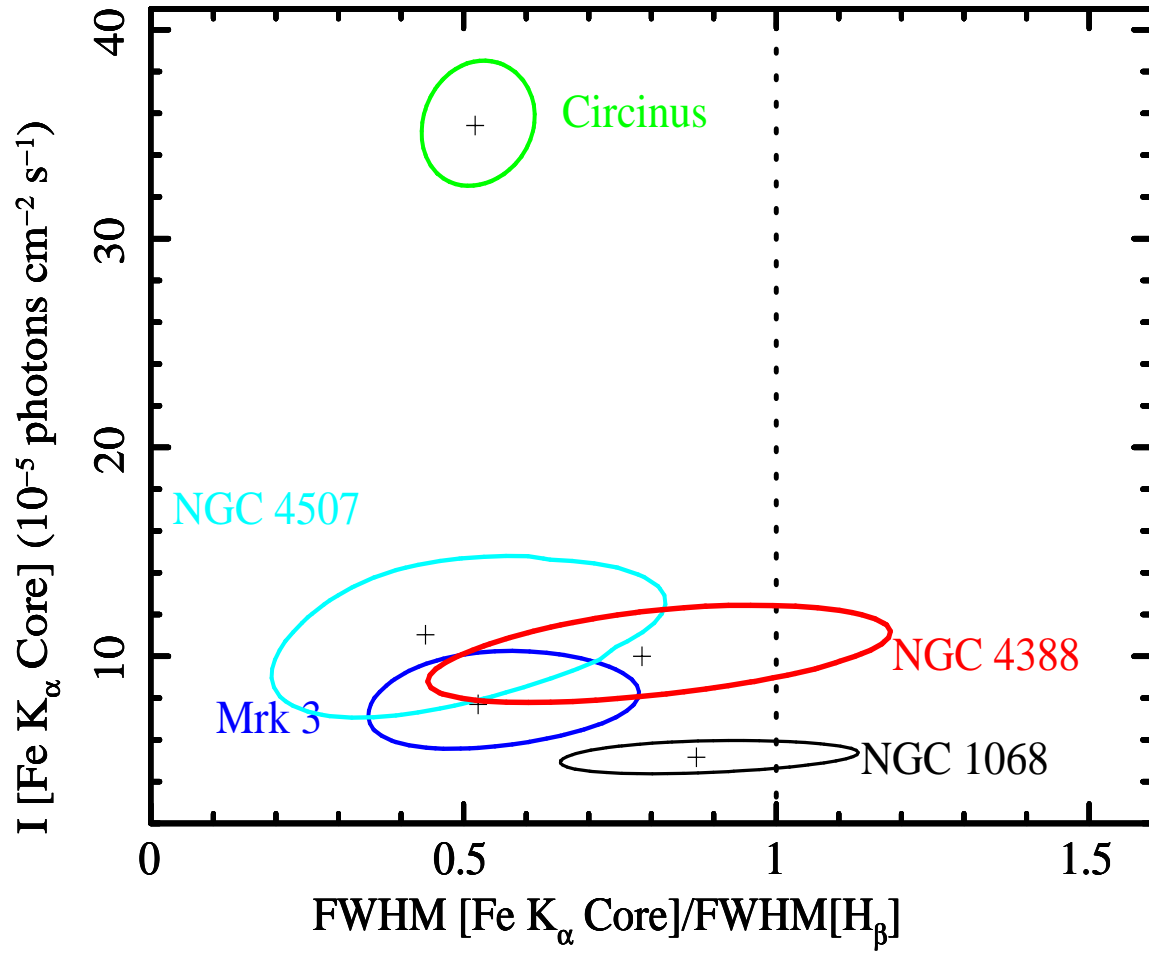


FIG. 3.— Joint 99% confidence contours of the Fe $K\alpha$ emission-line core intensity versus the ratio of the Fe $K\alpha$ FWHM to the $H\beta$ FWHM for 5 AGN that provided the values of $H\beta$ line FWHM from spectro-polarimetric observation (see text). For Circinus and NGC 4507, we used the FWHM of $H\alpha$ line as a surrogate for $H\beta$ FWHM. The vertical dotted lines correspond to a FWHM ratio of the pairs of emission lines equal to unity.

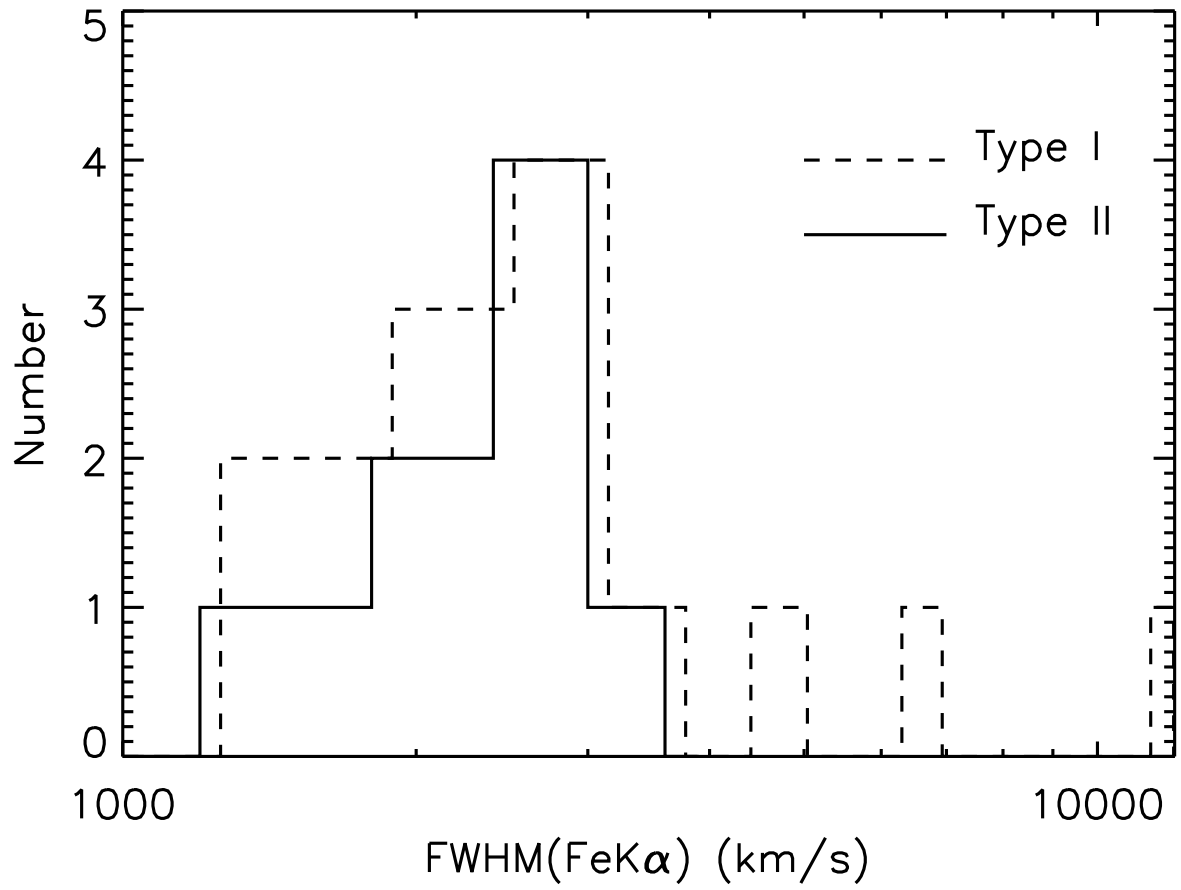


FIG. 4.— Distribution of the Fe K α line FWHM derived from those sources for which the best Fe K α line FWHM constraints were obtained. Dashed and solid lines correspond to the distribution for type I (see Paper I) and type II AGNs, respectively.

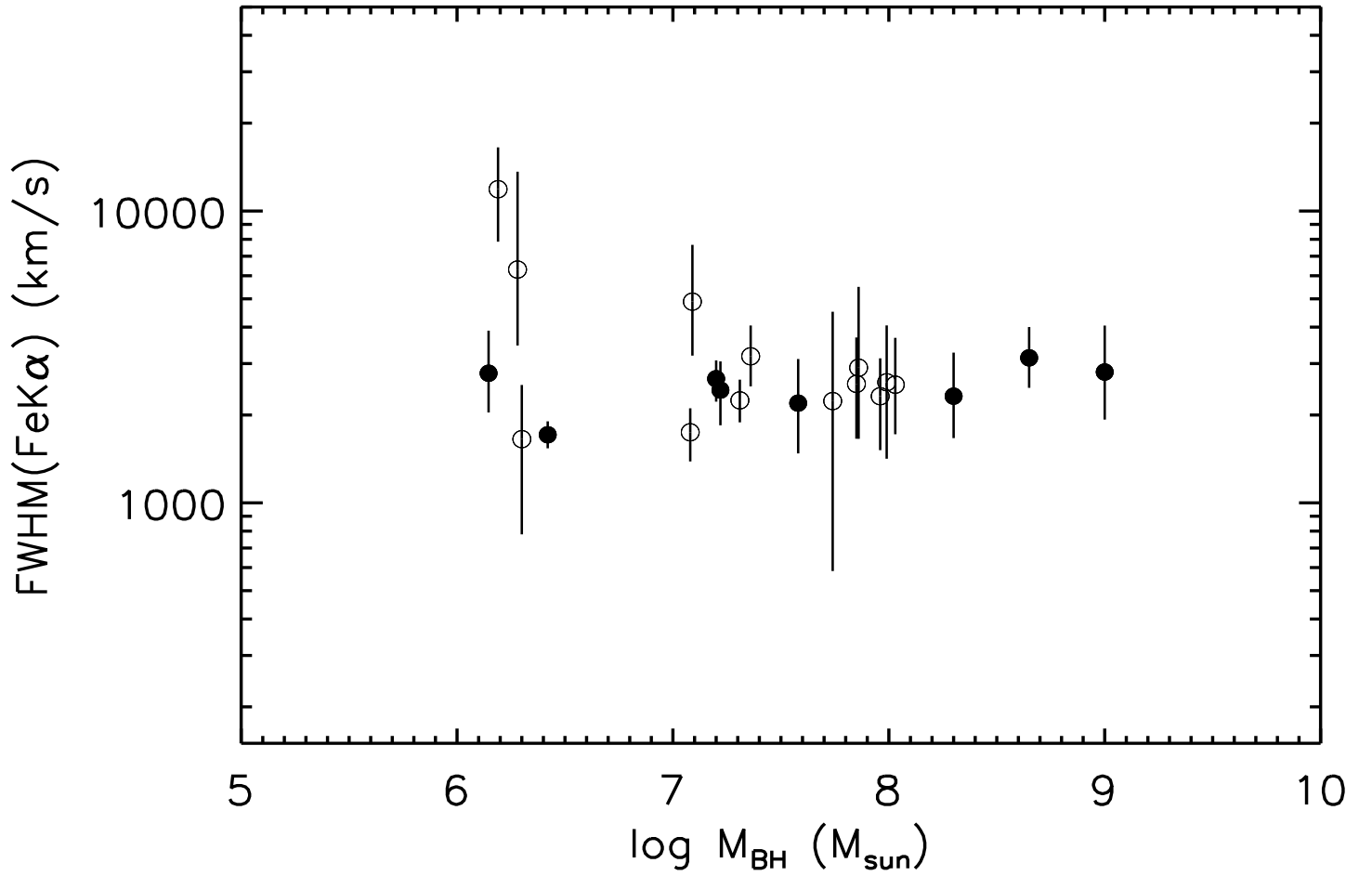


FIG. 5.— Fe K α emission-line FWHM versus the black hole mass. Solid circles denotes type II AGNs, and open circles correspond to the 13 type I sources shown in Figure 4. The statistical errors on the Fe K α line FWHM shown correspond to 68% confidence for three free parameters. It can be seen that while the black hole mass spans a range from 10^6 to 10^9 M_{\odot} , the Fe K α line FWHM remains nearly constant, clustering at ~ 2000 - 3000 km s^{-1} (see text).

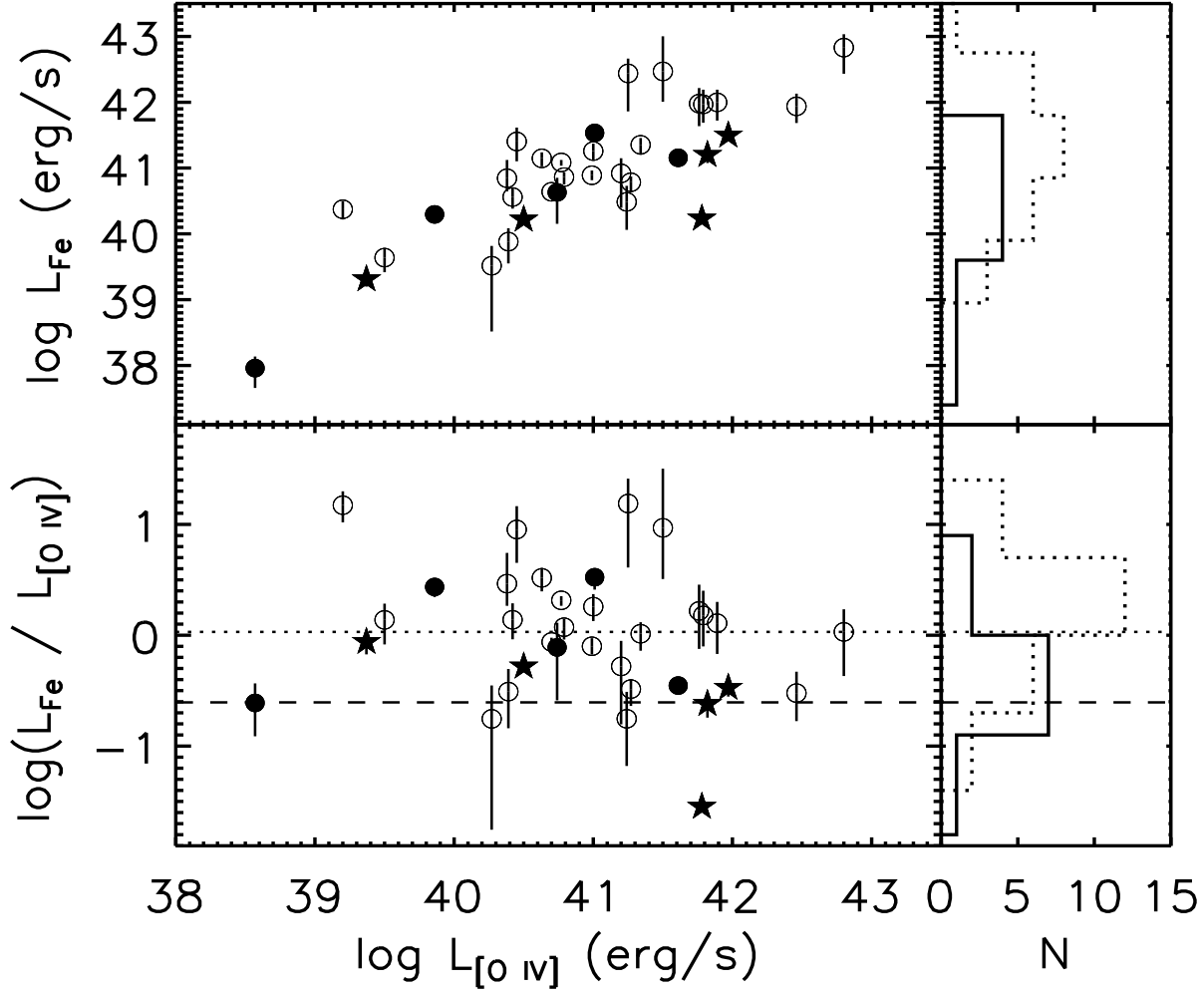


FIG. 6.— The [O IV] $\lambda 25.89\mu\text{m}$ line luminosity versus the Fe K α core emission-line luminosity (upper panel). The lower panel shows the [O IV] $\lambda 25.89\mu\text{m}$ line luminosity versus the ratio of Fe K α luminosity to [O IV] luminosity. Both solid and open circles have the same meaning as in Figure 5, while Compton-thick AGNs are distinguished by the solid stars. The right-hand panel is the distribution of the Fe K α luminosity and the ratio of $L_{\text{Fe}}/L_{[\text{OIV}]}$, respectively. The statistical errors on the Fe K α line luminosity correspond to 68% confidence ($\Delta C = 3.506$, or 0.989 , depending on whether there were three parameters or one parameter free respectively). The dotted and dashed horizontal lines represent the means of the $L_{\text{Fe}}/L_{[\text{OIV}]}$ for Liu & Wang (2010)'s type I and type II subsamples, respectively.

TABLE 1
OBSERVATION LOG OF THE *Chandra* HEG SAMPLE IN THIS WORK

Source	z	SeqNum	ObsID	Exposure (ks)	ObsDate
NGC 4945	0.001878	700981	4899	78.6	2004-05-28
		700981	4900	95.8	2004-05-29
Circinus	0.001448	700046	374	7.3	2000-06-15
		700268	62877	61.4	2004-06-02
		700853	4770	56.1	2004-06-02
		700854	4771	60.2	2004-11-28
NGC 6240	0.024480	701324	6908	159.0	2006-05-16
		701324	6909	143.0	2006-05-11
NGC 1068	0.003793	700004	332	46.3	2000-12-04
		701591	9148	80.9	2008-12-05
		701591	9149	91.2	2008-11-19
		701591	10815	19.4	2008-11-20
		701591	10816	16.4	2008-11-18
		701591	10817	33.2	2008-11-22
		701591	10829	39.1	2008-11-30
		701591	10830	43.6	2008-12-03
		701592	9150	41.8	2008-11-27
		701592	10823	35.1	2008-11-25
		Mrk 3	0.013509	700178	873
NGC 4507	0.011801	700340	2150	139.8	2001-03-15
Centaurus A	0.001825	700216	1600	47.5	2001-05-09
		700217	1601	52.2	2001-05-21
NGC 4388	0.008419	701717	9276	172.8	2008-04-16
		701717	9277	99.6	2008-04-24
NGC 4258	0.001494	701543	7879	152.9	2007-10-08
		701543	7880	60.0	2007-10-12
		701543	9750	107.1	2007-10-14
NGC 1275	0.017559	700005	333	27.4	1999-10-10
		700201	428	25.0	2000-08-25

TABLE 2
PARAMETERS OF THE CORE Fe K α LINE EMISSION FROM *Chandra* (HEG) DATA

Source	$F_{2-10 \text{ keV}}$	E	EW	FWHM(Fe K α)	I(Fe K α)	L(Fe K α)	FWHM (H β)	M_{BH}	$L_{[\text{OIV}]}$
(1)	(2)	(keV) (3)	(eV) (4)	(km s $^{-1}$) (5)	(6)	(7)	(km s $^{-1}$) (8)	(9)	(10)
NGC 4945(2)*	2.6	6.389 $^{+0.007}_{-0.008}$	840 $^{+164}_{-191}$	2780 $^{+1110}_{-740}$	2.6 $^{+0.5}_{-0.6}$	39.31 $^{+0.08}_{-0.11}$...	6.2	39.37
Circinus(4)*	16.0	6.396 $^{+0.002}_{-0.001}$	1673 $^{+91}_{-83}$	1710 $^{+190}_{-170}$	35.4 $^{+1.9}_{-1.8}$	40.22 $^{+0.02}_{-0.02}$	3300 †	6.1	40.50
NGC 6240(2)*	2.9	6.394 $^{+0.009}_{-0.009}$	333 $^{+96}_{-79}$	2810 $^{+1240}_{-880}$	1.2 $^{+0.3}_{-0.3}$	41.20 $^{+0.10}_{-0.12}$...	9.0	41.82
NGC 1068(10)*	5.6	6.402 $^{+0.003}_{-0.003}$	779 $^{+72}_{-76}$	2660 $^{+410}_{-440}$	5.2 $^{+0.5}_{-0.5}$	40.23 $^{+0.04}_{-0.04}$	3030	7.2	41.78
Mrk 3*	6.3	6.396 $^{+0.007}_{-0.008}$	612 $^{+123}_{-104}$	3140 $^{+870}_{-660}$	7.7 $^{+1.5}_{-1.3}$	41.50 $^{+0.08}_{-0.08}$	6000	8.6	41.97
NGC 4507	27.9	6.395 $^{+0.007}_{-0.006}$	114 $^{+21}_{-26}$	2200 $^{+910}_{-720}$	11.0 $^{+2.0}_{-2.5}$	41.53 $^{+0.07}_{-0.11}$	5000 †	7.6	41.01
Centarus A(2)	310.8	6.396 $^{+0.005}_{-0.007}$	45 $^{+9}_{-8}$	2320 $^{+950}_{-650}$	26.4 $^{+5.2}_{-5.0}$	40.30 $^{+0.08}_{-0.09}$...	8.3	39.86
NGC 4388(2)	23.1	6.393 $^{+0.004}_{-0.004}$	169 $^{+24}_{-21}$	2430 $^{+620}_{-590}$	10.0 $^{+1.4}_{-1.2}$	41.16 $^{+0.06}_{-0.06}$	3100	7.2	41.61
NGC 4258(3)	9.0	6.4 (fixed)	14 $^{+9}_{-9}$	100 (fixed)	0.2 $^{+0.1}_{-0.1}$	37.96 $^{+0.18}_{-0.30}$...	7.6	38.57
NGC 1275(2)	30.2	6.4 (fixed)	19 $^{+14}_{-15}$	100 (fixed)	0.6 $^{+0.4}_{-0.4}$	40.63 $^{+0.22}_{-0.48}$...	8.5	40.74

NOTE. — Results from *Chandra* HEG data, fitted with a absorbed power law plus Gaussian emission-line model in the 3–10 keV band. All parameters are quoted in the source rest frame. Statistical errors are for the 68% confidence level for three free parameters in the Gaussian component of the model (corresponding to $\Delta C=3.506$). For NGC 4258 and NGC 1275, the 1σ statistical errors are for one free parameter, corresponding to $\Delta C=0.989$. Col.(1): Source Name, whilst parentheses show the number of the observations used to produce the time-averaged spectrum. All HEG observations were in the *Chandra* public archives as of 2010 Aug 1 (see Section 2). *Compton-thick AGN; Col.(2): The observed 2–10 keV flux in units of 10^{-12} ergs cm^{-2} s^{-1} ; Col.(3): Gaussian line centroid energy; Col.(4): Emission line equivalent width; Col.(5): Full width half maximum of the Fe K α , rounded to 10 km s^{-1} . Col.(6): Emission-line intensity in units of 10^{-5} photons cm^{-2} s^{-1} . Col.(7): The logarithm of Fe K α line luminosity in units of ergs s^{-1} ; Col.(8): Full width half maximum of the broad polarized H β line, refers to Oliva et al. 1998; Nishiura & Taniguchi 1998; Moran et al. 2000; Young et al. 1996. † Broad polarized H α line. Col.(9): Black hole mass, refers to: Greenhill, Moran, & Herrnstein (1997); Bian & Gu (2007); Tecza et al. (2000); Tremaine et al. (2002); Marconi et al. (2001); Woo & Urry (2002). Col.(10): Logarithm of the [O IV] emission line luminosity, refers to: Liu & Wang (2010); Meléndez et al. (2008b).